Differential phase-contrast microscope with a split detector for the readout system of a multilayered optical memory

Y. Kawata, R. Juškaitis, T. Tanaka, T. Wilson, and S. Kawata

A transmission differential phase-contrast microscope with a split detector is used as a readout system for a multilayered three-dimensional optical memory. The system is applicable to data recorded as refractive-index changes. The system is compact and easy to use. The three-dimensional optical transfer function for the system is derived. This shows that the spatial bandwidth of the system is the same as that of a conventional microscope with incoherent illumination but with much improved contrast. Six layers of information are recorded in a photopolymer and are read out with little cross talk and high contrast.

Key words: Optical memory, photorefractive, differential phase-contrast microscope, three-dimensional optics, nonlinear optics, holographic memory. © 1996 Optical Society of America

1. Introduction

Multilayered optical memories have been recently developed.[1–7] In these memories, data are recorded throughout the volume of the medium as well as in the plane. If, for example, we record 10 or 20 layers of data, we can achieve 10 or 20 times higher storage than that with current optical memories, such as compact disks or magneto-optic disks. Multilayered optical memories are therefore important because they can overcome the limitations of the density of current optical memories.

Strickler and Webb, for example, have already succeeded in recording 25 layers in a volume material.[2] We, on the other hand, have succeeded in developing an optical storage card with 30 recorded layers.[6] The recording density was 25 Gbits/cm^2, the distance between layers was 7 μm, and the distance between bits in the plane was 2 μm.

Photopolymers[2,3,6] and photorefractive crystals[3–5] have been used as the data-recording medium. In both cases the bit data were recorded as refractive-index changes, and so the readout system needs to be particularly sensitive to these changes. Strickler and Webb used a Nomarski differential interference-contrast microscope to read their data,[2] whereas Kawata and co-workers used a nondifferential Zernike phase-contrast microscope.[3–6]

In this paper we describe an alternative readout system that uses a scanning differential phase-contrast microscope with a split detector.[8–11] This microscope is sensitive to small variations in phase and produces high-contrast images. The optical configuration is also compact and easy to align, which suggests that this approach may find use as a practical readout system for such three-dimensional (3-D) optical memories.

2. Imaging Properties of the Differential Phase-Contrast Readout System

Figure 1 shows the optical configuration of the scanning differential phase-contrast microscope with a split detector, which we used to read the data in our multilayered optical memory. The memory medium, in which the data bits have been recorded, is located at the focus of an objective lens. The details of the data-recording process are discussed in Section 3.

We now discuss 3-D image formation by using wave-vector analysis. The distribution of wave vectors in object space is given by[12,13]

$$U(\boldsymbol{\xi}) = P(\xi, \eta)\delta(\zeta - [\lambda^{-2} - (\xi^2 + \eta^2)]^{1/2}), \qquad (1)$$

where $\boldsymbol{\xi} = (\xi, \eta, \zeta)$ is a wave vector. $P(\xi, \eta)$ is a pupil

Y. Kawata, T. Tanaka, and S. Kawata are with the Department of Applied Physics, Osaka University, Suita, Osaka 565, Japan; R. Juškaitis and T. Wilson are with the Department of Engineering Science, University of Oxford, Parks Road, Oxford 0X1 3PJ, U.K.

Received 29 August 1995; revised manuscript received 2 January 1996.

0003-6935/96/142466-05$10.00/0

© 1996 Optical Society of America

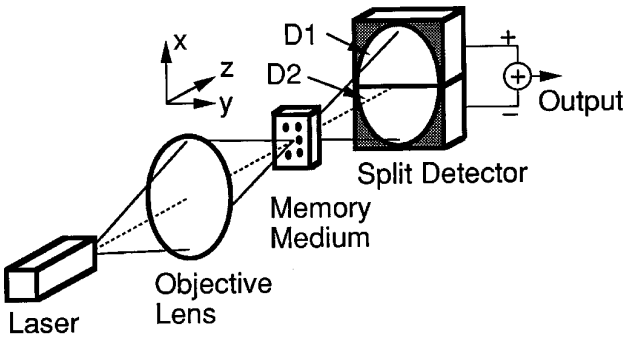

Fig. 1. Optical setup for a phase-contrast microscope with a split detector.

function of the objective lens, where

$$P(\xi, \eta) = \begin{cases} 1 & \text{if } \xi^2 + \eta^2 \le (\mathrm{NA}/\lambda)^2 \\ 0, & \text{otherwise} \end{cases}, \tag{2}$$

λ is the wavelength of the laser light used to read the data, and NA is the numerical aperture.

The light incident upon the recording medium is diffracted by the data bits. Suppose that incident light of wave vector $\boldsymbol{\xi}_0$ is diffracted by a spatial component of $\mathbf{p} = (p_x, p_y, p_z)$ and its wave vector is represented by $\boldsymbol{\xi}_d = (\xi_d, \eta_d, \zeta_d)$. $\boldsymbol{\xi}_d$ is related to $\boldsymbol{\xi}_0$ and $\mathbf{p}$ by

$$\boldsymbol{\xi}_d = \boldsymbol{\xi}_0 + \mathbf{p}, \tag{3}$$

which is essentially the Bragg condition.

The transmitted light and the diffracted light interfere and are detected at the detector plane. The intensity at $\boldsymbol{\xi}_d$ in the detector plane is described by the interference between the transmission and the diffraction:

$$\begin{aligned} \hat{I}_1(\boldsymbol{\xi}_d, \mathbf{p}; \mathbf{x}_s) &= |U(\boldsymbol{\xi}_d)\exp(j\boldsymbol{\xi}_d \cdot \mathbf{x}) + ja(\mathbf{p})\exp[j\mathbf{p} \cdot (\mathbf{x} - \mathbf{x}_s)] \\ &\quad \cdot U(\boldsymbol{\xi}_0)\exp(j\boldsymbol{\xi}_0 \cdot \mathbf{x})|^2 \\ &= [|U(\boldsymbol{\xi}_d)|^2 + |ja(\mathbf{p})U(\boldsymbol{\xi}_d - \mathbf{p})|^2] \\ &\quad - ja^*(\mathbf{p})\exp(j\mathbf{p} \cdot \mathbf{x}_s)U(\boldsymbol{\xi}_d)U(\mathbf{p} - \boldsymbol{\xi}_d) \\ &\quad + ja(\mathbf{p})\exp(-j\mathbf{p} \cdot \mathbf{x}_s)U^*(\boldsymbol{\xi}_d)U^*(\mathbf{p} - \boldsymbol{\xi}_d), \end{aligned} \tag{4}$$

where the coefficient j for the diffracted wave corresponds to the phase shift of $\pi/2$ generated in diffraction by phase objects and $a(\mathbf{p})$ is the amplitude of a spatial frequency of $\mathbf{p}$ of recorded data. The variables $\mathbf{x}$ and $\mathbf{x}_s$ are vectors for the position and scanning of the object, respectively. The relation of $U(\boldsymbol{\xi}) = U^*(-\boldsymbol{\xi})$ is used in the derivation.

The second and the third terms in Eq. (4) correspond to the imaging of the spatial frequency of $\mathbf{p}$ in a phase object. The distribution of the spatial frequency $\mathbf{p}$, which can be imaged with Eq. (4), is shown by the boldface curves in Fig. 2. The two arcs represent 3-D optical transfer functions (OTF's) for

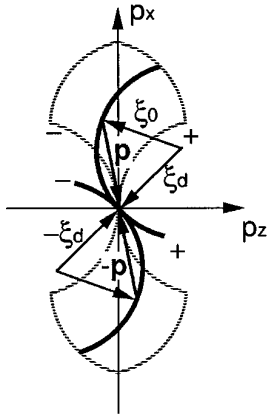

Fig. 2. Calculation process for the derivation of the 3-D transfer function. The two opposing arcs at the origin of the (p_x, p_z) coordinate, indicated by dashed curves, are the 3-D optical transfer functions for a phase object with coherent detection. The two arcs indicated by the heavy curves are also 3-D optical transfer functions for the point detector located at (ξ_d, ζ_d).

the point detector located at (ξ_d, ζ_d). The imaginary j means an OTF for a phase object.[12]

The signal $I_1(\mathbf{p})$ detected by detector D1 is given by

$$\begin{aligned} I_1(\mathbf{p}) &= \int D_1(\xi_d, \eta_d)[|U(\boldsymbol{\xi}_d)|^2 + |a(\mathbf{p})U^*(\mathbf{p} - \boldsymbol{\xi}_d)|^2]\mathrm{d}\xi_d\mathrm{d}\eta_d \\ &\quad + \int D_1(\xi_d, \eta_d)[-ja^*(\mathbf{p})\exp(+j\mathbf{p} \cdot \mathbf{x}_s) \\ &\quad \times U(\boldsymbol{\xi}_d)U(\mathbf{p} - \boldsymbol{\xi}_d) + ja(\mathbf{p})\exp(-j\mathbf{p} \cdot \mathbf{x}_s)U^*(\boldsymbol{\xi}_d) \\ &\quad \times U^*(\mathbf{p} - \boldsymbol{\xi}_d)]\mathrm{d}\xi_d\mathrm{d}\eta_d, \end{aligned} \tag{5}$$

where $D_1(\boldsymbol{\xi}_d)$ is a pupil function of detector D1,

$$D_1(\xi, \eta) = \begin{cases} 1 & \text{if } \xi^2 + \eta^2 \le r_D{}^2 \text{ and } \xi > 0 \\ 0, & \text{otherwise} \end{cases}, \tag{6}$$

and r_D is a radius of the sensitive area.

The signal detected from detector D2 is derived in the same way except that subscript 1 is replaced by 2:

$$\begin{aligned} I_2(\mathbf{p}) &= \int D_2(\xi_d, \eta_d)[|U(\boldsymbol{\xi}_d)|^2 \\ &\quad + |a(\mathbf{p})U^*(\mathbf{p} - \boldsymbol{\xi}_d)|^2]\mathrm{d}\xi_d\mathrm{d}\eta_d \\ &\quad + \int D_2(\xi_d, \eta_d)[-ja^*(\mathbf{p})\exp(+j\mathbf{p} \cdot \mathbf{x}_s) \\ &\quad \times U(\boldsymbol{\xi}_d)U(\mathbf{p} - \boldsymbol{\xi}_d) + ja(\mathbf{p})\exp(-j\mathbf{p} \cdot \mathbf{x}_s)U^*(\boldsymbol{\xi}_d) \\ &\quad \times U^*(\mathbf{p} - \boldsymbol{\xi}_d)]\mathrm{d}\xi_d\mathrm{d}\eta_d, \end{aligned} \tag{7}$$

$$D_2(\xi, \eta) = \begin{cases} 1 & \text{if } \xi^2 + \eta^2 \le r_D{}^2 \text{ and } \xi < 0 \\ 0, & \text{otherwise} \end{cases}. \tag{8}$$

Finally the signal from detector D2 is subtracted from that of detector D1. As a result, we get the

output signal:

$$I(\mathbf{p}) = I_1(\mathbf{p}) - I_2(\mathbf{p})$$
$$= 2\int D_1(\xi_d, \eta_d)[-ja^*(\mathbf{p})\exp(+j\mathbf{p}\cdot\mathbf{x}_s) \times U(\boldsymbol{\xi}_d)U(\mathbf{p}-\boldsymbol{\xi}_d) + ja(\mathbf{p})\exp(-j\mathbf{p}\cdot\mathbf{x}_s) \times U^*(\boldsymbol{\xi}_d)U^*(\mathbf{p}-\boldsymbol{\xi}_d)]\mathrm{d}\xi_d\mathrm{d}\eta_d, \quad (9)$$

where we have assumed that $D_1(\xi, \eta) = D_2(-\xi, \eta)$.

By using Eq. (9) we can derive the 3-D OTF. OTF($\mathbf{p}$) is given by

$$\mathrm{OTF}(\mathbf{p}) = \int D_1(\xi_d, \eta_d)[jU(\boldsymbol{\xi}_d)U(\mathbf{p}-\boldsymbol{\xi}_d) - jU^*(\boldsymbol{\xi}_d)U^*(\mathbf{p}-\boldsymbol{\xi}_d)]\mathrm{d}\xi_d\mathrm{d}\eta_d. \quad (10)$$

$D_1(\xi_d, \eta_d)U(\boldsymbol{\xi}_d)$ represents a half-shell ($\xi_d > 0$), and $D_1(\xi_d, \eta_d)U^*(\boldsymbol{\xi}_d)$ represents another half-shell ($\xi_d < 0$).

Figure 2 shows the calculation process of Eq. (10). Two opposing arcs at the origin of the p_x, p_z coordinate, which are indicated by dashed curves, are 3-D OTF's for a phase object with coherent detection. This 3-D OTF is the same as that of a conventional microscope with coherent illumination, which was derived by Streibl.[12] The two arcs indicated by boldface curves are also 3-D OTF's for the point detector located at (ξ_d, ζ_d). The 3-D OTF corresponds to that of a conventional microscope with oblique illumination. The signal detected by D1 is a summation of the signal obtained at the point (ξ_d, ζ_d).

Figure 3 shows the calculated 3-D OTF of a conventional microscope with incoherent illumination, and in particular that of a phase-contrast microscope with a split detector. Figure 3(a) shows the p_x–p_z plane. The sign of OTF(p_x, 0, p_z) is positive for $p_x > 0$ and negative for $p_x < 0$. The band limit of p_z is $(1 - \mathrm{NA}^2)^{1/2}/\lambda$ and the bandwidth of p_x is $2\mathrm{NA}/\lambda$. The band limit is the same as that of the 3-D OTF of a conventional microscope with incoherent illumination.[12,13] Low frequencies of the 3-D OTF are suppressed for the phase-contrast microscope images shown in Figs. 3, whereas they are not suppressed for those of a conventional microscope, and in particular the dc bias component of the phase-contrast microscope is absolutely eliminated. The absence of the bias component yields a high-contrast image of the phase object.

The p_y–p_z plane of a 3-D OTF is 0 for all spatial components. The spatial components of $p_y = 0$ cannot be imaged with this readout system.

Figure 3(b) shows p_x–p_y plane of a 3-D OTF. The sign of OTF(p_x, p_y, 0) is positive for $p_x > 0$ and negative for $p_x < 0$. The band limit of the OTF for the direction along the p_x axis is $2\mathrm{NA}/\lambda$. This band limit is same as that of a conventional incoherent-illumination microscope.

The band limit of the OTF is the same as that of a conventional microscope with incoherent illumination; nevertheless a half-pupil detector is used for the detection. The resolution, especially the axial resolution of the phase-contrast microscope, is not worse than that of Zernike's phase-contrast microscope, which is usually used for the readout of a multilayered optical memory.[3,4] The contrast of an image obtained with the phase-contrast microscope is extensively improved compared with that of Zernike's phase-contrast microscope[3] because the nondiffracted components are completely eliminated by the subtraction of signals between two detectors. The readout system is therefore sensitive to small phase changes.

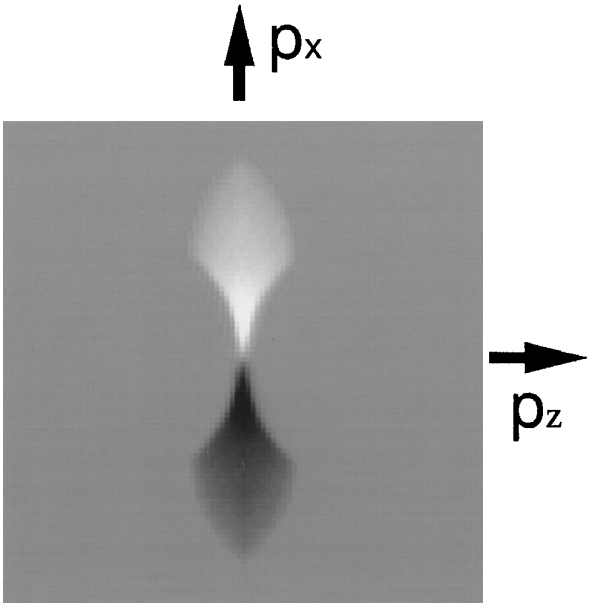

(a)

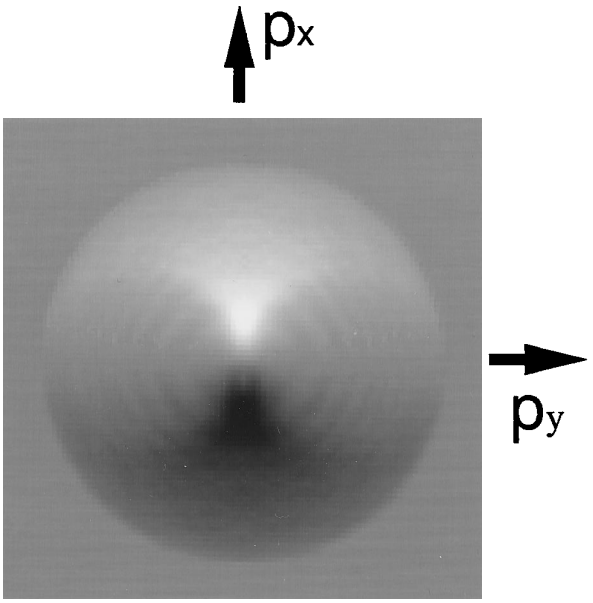

(b)

Fig. 3. 3-D OTF: (a) cross section of the p_x–p_z plane, and (b) cross section of the p_x–p_y plane.

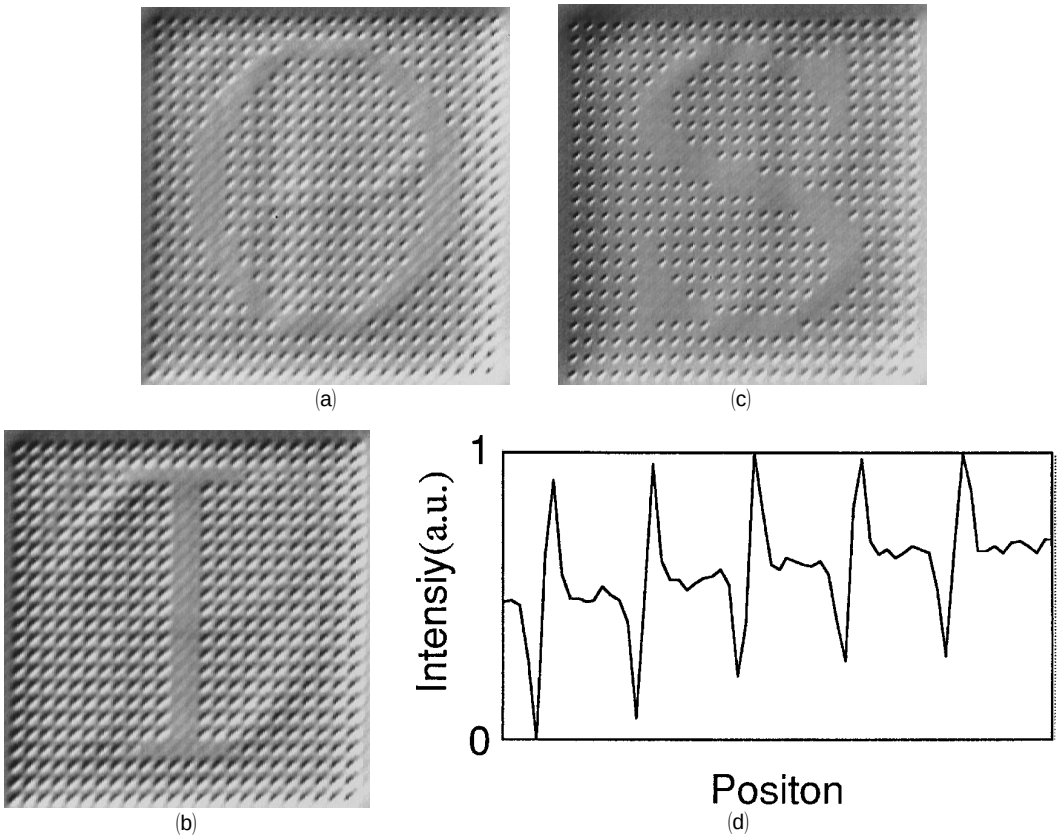

Fig. 4. Experimental results of the readout of the data: (a) the first layer, O in a square is formed by the bit sequence; (b) the fourth layer, formed with I; (c) the sixth layer, with S; and (d) a cross section of 5 bits along the diagonal of (c).

3. Experimental Results

We used the transmission differential phase-contrast microscope system shown in Fig. 1 to read our 3-D optical memory. We elected to use a 670-nm semiconductor laser (10 mW) as the light source because this gave adequate spatial resolution and our photopolymer is relatively insensitive to this wavelength. A high-aperture objective lens (Zeiss Neofuar, oil immersion, NA = 1.3, 100× magnification) was used together with mechanical object scanning.

Figure 4 shows examples of the readout data obtained with this system. The photopolymer memory in this case consisted of six layers into which the capital letters O, P, T, I, C, and S had been encoded sequentially. Figure 4(a) shows the first layer of the recorded data, the capital letter O in a square. The bit data are clearly seen in Fig. 4(a), and there is little cross talk from other layers. Figure 4(b) shows the fourth layer of recorded data, the capital letter I. Again no cross talk is observed. Finally, Figure 4(c) shows the sixth layer, the letter S. The axial separation between neighboring layers was 15 μm, and the lateral distance between neighboring bits in the plane was 2 μm.

Figure 4(d) shows a line scan of 5 bits along a diagonal of the readout data shown in Fig. 4(c). Because the differential phase-contrast image signal is bidirectional, it is necessary to add a constant offset before the data can be displayed. It is also possible to amplify the signal and in this way to obtain high-contrast images that use the full dynamic range of the display. We note that this is an important advantage of our approach. We have the freedom to expand the contrast in a simple manner.

The photopolymer memory medium we used was a monomer mixture composed of a methacryl compound and an allyl compound with benzil as an initiator and Michler's ketone as a dye sensitizer.[14] The methacryl compound polymerizes faster than the allyl compound when illuminated with light. This causes the refractive index to increase from $n \simeq 1.5$ to $n \simeq 1.6$.

The photopolymerizable solution was sandwiched between a microscope slide and a microscope cover glass (thickness 170 μm) to prevent oxygenation of the photopolymer. The spacers between the slide and the cover glass were also made of cover slips of ~1-mm thickness.

The photopolymer was initially uniformly exposed with white light for 40 min to polymerize the material partially. We can control the nonlinearity of recording in the photopolymer by adjusting the preexposure time. Some monomers are polymerized by the pre-exposure. As a result, the photopolymer solution becomes like a gel. The diffusion length of monomers in the gel becomes shorter than that in the solution, because monomers cannot move

freely in the gel. The longer the exposure time, the shorter the diffusion length. The short diffusion length of monomers corresponds to high-pass filtering properties for spatial frequencies of the incident light distribution, because it is difficult to record an interference fringe if the pitch is much longer than the diffusion length of the monomers.

In order to write the data, the photopolymer is placed on a computer-controlled x–y–z microscope stage (0.02-μm resolution). A 5-mW argon-ion laser, 488-nm wavelength, was used as the light source, which was focused onto the photopolymer by an objective lens (Carl Zeiss Axiophot, NA = 1.0, oil immersion, 40× magnification). An exposure time of 60 ms per point was used. At the focused spot, methacryl compounds photopolymerize because of their fast photopolymerization property. Allyl compounds, on the other hand, do not photopolymerize because the speed of photopolymerization of allyl compounds is slower than that of methacryl compounds.

As a result, only methacryl compounds are polymerized at the focused spot and the allyl compounds are pushed away, leaving a high-refractive-index region. We then record the data in the medium by scanning a focused spot in three dimensions with an exposure time of 60 ms at each data point.

4. Discussion and Conclusion

We have calculated the 3-D OTF for the differential phase-contrast microscope with a split detector and have found that its region of support is comparable with that of the conventional microscope with incoherent illumination. The 3-D OTF of the readout system, however, possesses a high-pass filtering property, which enhances the data readout. In addition, because subtracting the signals from the two detectors has illuminated the dc level, a high degree of contrast enhancement is possible, much higher than we were able to achieve with the Zernike system.[3,6]

The differential phase-contrast microscope with a split detector that we have described is compact and easy to use. The optical alignment is also simple: all that is required is to place a split detector behind the photopolymer. A condenser lens is not required. Furthermore no special phase-contrast-type objective is required. The system simply uses an ordinary microscope objective, and so the same lens may be used for both writing and reading the data. This has implications for rewritable optical memory systems.

The confocal optical system may also be used to read the data with high contrast because it employs a pinhole placed in front of the detector, which greatly attenuates any light scattered from out-of-focus data.[3] However, the alignment of confocal systems in transmission is difficult and is likely to limit their practical use. Further, spherical aberration caused by the deep focus into the material is likely to be an additional problem that will reduce both the resolution and the signal-to-noise ratio, because both a focusing objective and a collecting lens suffer the spherical aberration.

The large change of refractive index leads a high signal-to-noise ratio if only one bit is recorded in a medium, and it also yields large cross talk from other layers in the 3-D memory. We experimentally decided the optimal refractive-index change to separate each layer clearly. It needs a theoretical discussion on the optimal change of refractive index and signal-to-noise ratio or error rate.

The speed of data readout of our prototype system is limited by the speed of our mechanical scanning stage. However, it would be relatively straightforward to replace this with faster beam scanning, or to rotate the memory material quickly, as is done currently in conventional memory systems.

This research was sponsored by a grant in aid from the International Collaboration Program of The Ministry of Education, Science, Sports, and Culture, Japan, and by the Casio Science Promotion Foundation.

References

1. D. A. Parthenopoulos and P. M. Rentzepis, "Three-dimensional optical storage memory," Science **245,** 843–845 (1989).
2. J. H. Strickler and W. W. Webb, "Three-dimensional optical data storage in refractive media by two-photon point excitation," Opt. Lett. **16,** 1780–1782 (1991).
3. S. Kawata, T. Tanaka, Y. Hashimoto, and Y. Kawata, "Three-dimensional confocal optical memory using photorefractive materials," in *Photopolymers and Applications in Holography, Optical Data Storage, Optical Sensors, and Interconnects,* R. A. Lesard, ed., Proc. SPIE **2042,** 314–325 (1993).
4. Y. Kawata, H. Ueki, Y. Hashimoto, and S. Kawata, "Three-dimensional optical memory with a photorefractive crystal," Appl. Opt. **34,** 4105–4110 (1995).
5. H. Ueki, Y. Kawata, and S. Kawata, "Three-dimensional optical bit memory recording and reading with a photorefractive crystal: analysis and experiment," Appl. Opt. **35,** 2457–2465 (1996).
6. T. Tanaka and S. Kawata, "Three dimensional optical card storage with thirty recording layers," presented at the Conference on Laser and Electro-Optics/Pacific Rim '95, Chiba, Japan, 11–14 July 1995.
7. K. A. Rubin, H. J. Rosen, W. W. Tang, T. Imaino, and T. Strand, "Multilevel volumetric optical storage," in *Optical Data Storage,* Vol. 10 of 1994 OSA Technical Digest Series (Optical Society of America, Washington, D.C., 1994), pp. 108–114.
8. T. Wilson and C. J. R. Sheppard, *Theory and Practice of Scanning Optical Microscopy* (Academic, London, 1984).
9. T. Wilson, "Confocal microscopy," in *Confocal Microscopy,* T. Wilson ed. (Academic, London, 1990), pp. 1–64.
10. D. K. Hamilton and C. J. R. Sheppard, "Differential phase contrast in scanning optical microscopy," J. Microsc. **133,** 27–39 (1984).
11. C. J. Cogswell and C. J. R. Sheppard, "Confocal differential interference contrast (DIC) microscopy: including a theoretical analysis of conventional and confocal DIC imaging," J. Microsc. **165,** 81–101 (1992).
12. N. Streibl, "Three-dimensional imaging by a microscope," J. Opt. Soc. Am. A **2,** 121–127 (1985).
13. O. Nakamura and S. Kawata, "Three-dimensional transfer-function analysis of the tomographic capability of a confocal fluorescence microscope," J. Opt. Soc. Am. A **7,** 522–526 (1990).
14. H. Tanigawa, T. Ichihashi, and A. Nagata, "Hologram recording on multicomponent monomer materials," Kogaku **20,** 227–231 (1991).